

Supporting Information

“Dynamics of the bacterial flagellar motor with multiple stators”

Giovanni Meacci and Yuhai Tu

I. TORQUE-SPEED CURVE MEASUREMENT

The measurement of the torque-speed curve is usually done by fixing the cell to a glass slide and tethering a polystyrene bead to the flagellar hook. An optical trap monitor the rotational speed of the bead and the motor torque is calculated from $\tau = (\xi_L + \xi_R)\omega \approx \xi_L\omega$, where ξ_R is the drag coefficient due to the internal friction in the motor, ξ_L is the bead drag coefficient, and ω is the angular velocity. The torque-speed curve is then obtained changing ξ_L by varying the bead size [1] or the viscosity of the external medium. An alternative method is to tether a cell to a glass coverslip by one of its shortened flagellar filament and expose the cell to a rotating electric field [2]. Then the motor is broken spinning the cell backward. The difference between the cell body speeds before and after the broke of the motor, at the same value for the external applied torque, is proportional to the motor torque.

II. HOOK SPRING COMPLIANCE

Fig. S1 shows the compliance curve F (motor torque versus angular displacement $\theta - \theta_L$) similar to the experimental one [3]. The following expression is used in our simulations:

$$F(x) = \kappa_0 x + \Delta x (\kappa_1 - \kappa_0) \log[1 + \exp((x - x_0)/\Delta x)], \quad (1)$$

with $x \equiv \theta - \theta_L$, κ_0 the spring constant a low load, $\kappa_1 (\gg \kappa_0)$ the spring constant a high load. At both low and high loads the spring behaves linearly with different spring constants κ_0 and κ_1 respectively. Δx is the angular displacement interval of the non linear region centered around the turning point x_0 . For the values of these parameters see Tab. S1.

III. DISTRIBUTION FUNCTIONS OF t_m AND t_w

Fig. S2 shows the distribution functions for t_m and t_w at different values of the load for the case $N=1$. Fig. S2(a) shows the average waiting and moving times. The arrows labeled with

the letter (b), (c), and (d) indicate the points (i.e. the speed values) where the probability distributions for t_m and t_w are shown in Fig. S2 (b), (c), and (d) respectively. The averaged waiting-time decreases slightly with the speed, while the averaged moving-time decreases by four orders of magnitude. The two time scales crossover at a speed around 170Hz, which naturally defines two regimes: i) $\langle t_w \rangle \ll \langle t_m \rangle$ and ii) $\langle t_w \rangle \gg \langle t_m \rangle$. The crossover speed corresponds roughly to ω_n .

Figs. S2(b), (c), and (d) show the differences in the distribution functions for t_m and t_w at high, medium, and low load respectively. The waiting times are exponentially distributed because the waiting time interval is determined by independent chemical transitions, i.e., by Poisson processes. The average waiting time thus depends on the stator jump rate k , which varies between two constants k_+ and k_- (except for extreme high load where $k = 0$): $\langle t_w \rangle \propto 1/k$. This explains why the averaged waiting time only weakly depends on the load. At low load, premature jumps are rare and the average angular movement δ_m is determined by a single stator jump and has a peaked distribution centered around δ_0/N . This explains the peaked distribution for t_m at low load, as shown in Fig. S2(b). At medium load, both $\langle t_m \rangle$ and the value of t_m corresponding to the peak of the distribution increase, as shown in Fig. S2(c). At high load, the t_m distribution develops a flat region for shorter time intervals, as shown in Fig. S2(b). This is a consequence of the decreasing slope of the total potential felt by the rotor on the positive force side. As a result, fluctuations of the rotor angle θ due to thermal noise increase, which leads to many short moving time intervals.

IV. DEPENDENCE OF THE TORQUE PLATEAU REGION ON K_+ AND δ_c

In order to understand the origin of the torque plateau region, we have studied the dependence of ω_n on the ratio $r \equiv k_+/k_-$ and on the cutoff δ_c for the case $N=8$ (similar results have been obtained for different values of N). We define ω_n as the speed value at which the torque decreases 10% from its value at stall. The size of the plateau regime is characterized by the following quantity:

$$\Sigma = \omega_n/\omega_{max}. \quad (2)$$

Fig. S3(a) shows the torque-speed curves for $N= 8$ and for two different values of r : $r = 0$ and $r = 1.2$. For $r = 0$ the torque, after a small plateau, decreases linearly with the speed.

Increasing r , ω_n increases and the torque-speed curve increase its concavity. In Fig. S3(b), Σ increases from 0.3 to 0.6 as r increases from 0.05 to 1. This corresponds to the values of r that can produce a well defined shoulder and at the same time maintain the independence of ω_{max} on N , i.e. $|\Delta| < 1$ (see Fig. 4(b) in the main text).

Fig. S3(c) shows four torque-speed curves for different values of the cutoff δ_c . Starting from the value used in the main text, i.e. $\delta_c = \delta_0$, ω_n increases with δ_c . In particular, Σ increases significantly from $\delta_c = \delta_0$ to $\delta_c = 3\delta_0$, at which the plateau size (ω_n) reaches a value slightly bigger than 60% of the maximum speed (Fig. S3(d)).

In conclusion the extension of the torque plateau region increases with the value of rate k_+ and the cutoff δ_c , in consistent with our theory.

V. ROBUSTNESS OF THE RESULTS AGAINST DIFFERENT ROTOR-STATOR POTENTIALS AND LOAD-ROTOR FORCES

In order to verify the independence of our results on the specifics of the rotor-stator potential, we studied our model with asymmetric potentials and a smoothed symmetric potential with a parabolic bottom (instead of the V-shaped bottom). In the asymmetric case, the slope τ_+ of the left branch of the potential is much smaller than the slope τ_- of the right branch, similar to the potential used in [4] (see the values used for τ_+ and τ_- in Tab. S1). Our model with the asymmetric potential yields qualitatively similar results as with the symmetric potential used in the main text. In particular, the maximum speeds near zero load are independent of the number of stators (see Fig. S4) provided the stator jumping rates satisfy: $k_-/k_+ \gg \tau_-/\tau_+$. Such a requirement can be understood intuitively in the following way. Given the condition $\tau_- \gg \tau_+$, the force equilibrium (waiting phase) is achieved by having one stator spending part of its time dragging the rotor while all the other stators are pulling the rotor. The waiting period ends when this dragging stator jumps with a rate that depends on the fractions of time it spends on the two sides of the potential, which depend on the ratio τ_-/τ_+ . Therefore, the condition that the maximum speed is dominated by k_- (instead of k_+) has to be weighted by the ratio τ_-/τ_+ .

We have also studied a “semi-parabolic” potential $V^P(\Delta\theta \equiv \theta - \theta_L)$ (see insert in Fig. S5)

defined as:

$$V^P = \begin{cases} \tau_0[|\Delta\theta| - (\Delta\theta_0/4)] & \text{if } |\Delta\theta| > \Delta\theta_0/2, \\ \tau_0\Delta\theta^2/\Delta\theta_0 & \text{if } |\Delta\theta| < \Delta\theta_0/2, \end{cases} \quad (3)$$

where τ_0 is the positive slope of the symmetric potential, and $\Delta\theta_0$ is the angular interval of the parabolic region centered around the bottom of the potential. Correspondingly, the chemical rate is a continuum function of $\Delta\theta$:

$$k(\Delta\theta) = k_+ + (k_- - k_+)/[1 + \exp(-(\Delta\theta)/\Delta\theta_0)] \quad (4)$$

Fig. S5 shows the torque-speed curves for $N = 1, 2, \dots, 8$. The curves show the same characteristics as for the V-shaped potential shown in the main text. The plateau region is a little wider. This is due to the change of the slope near the potential bottom. A lower value of the slope slows down the motion of rotor, increasing the premature jump probability before it reaches the bottom.

Next, we considered different forms of the force function F between the load and the rotor. Fig. S6 shows torque-speed curves for two cases: with and without a spring between the load and the rotor for different ratio k_+/k_- . The case with spring between the load and the rotor is studied in the main text; the case without spring corresponds to infinite spring constant (rigid connection between load and rotor) with the following equation for the rotor:

$$\frac{d\theta}{dt} = -\frac{1}{\xi_R + \xi_L} \frac{\partial V}{\partial \theta} + \sqrt{2k_B T / (\xi_R + \xi_L)} \alpha(t). \quad (5)$$

Contrary to the model proposed in [4], the concavity of the torque-speed curve does not depend on the strength of the hook spring: the torque-curves are almost identical with and without spring. Instead, the concavity of the torque-speed curve depends on the ratio of the jump rates k_+/k_- , and also on the cutoff δ_c as shown before in Fig. S3. In particular, as shown in Fig. S6, for $k_+ = 0$ the concavity is zero, and it increases as the ratio k_+/k_- increases.

-
- [1] Sowa, Y. Hotta, H. Homma, M. and Ishijima, A. (2003) Torque-speed Relationship of the Na^+ -driven Flagellar Motor of *Vibrio alginolyticus*. *J. Mol. Biol.* **327**, 1043-1051.
- [2] Berg, H. C. and Turner, L. (1993) Torque generated by the flagellar motor of *Escherichia coli*. *Biophysical J.* **65**, 2201-2216.
- [3] Block, S. M. Blair, D. and Berg, H. C. (1989) Compliance of bacterial flagella measured with optical tweezers. *Nature* **338**, 514-517.
- [4] Xing, J. Bai, F. Berry, R. and Oster, G. (2006) Torque-speed relationship of the bacterial flagellar motor. *Proc. Nat. Acad. Sci. USA* **103**, 1260-1265.
- [5] Berg, H. C. (2003) The rotatory motor of bacterial flagella. *Annu. Rev. Biochem.* **72**, 19-54.
- [6] Thomas, D. R. Francis, N. R. Xu, C. and DeRosier, D. J. (2006) The Three-Dimensional Structure of the Flagellar Rotor from a Clockwise-Locked Mutant of *Salmonella enterica* Serovar Typhimurium. *J. Bacteriol.* **188**, 7039-7048.

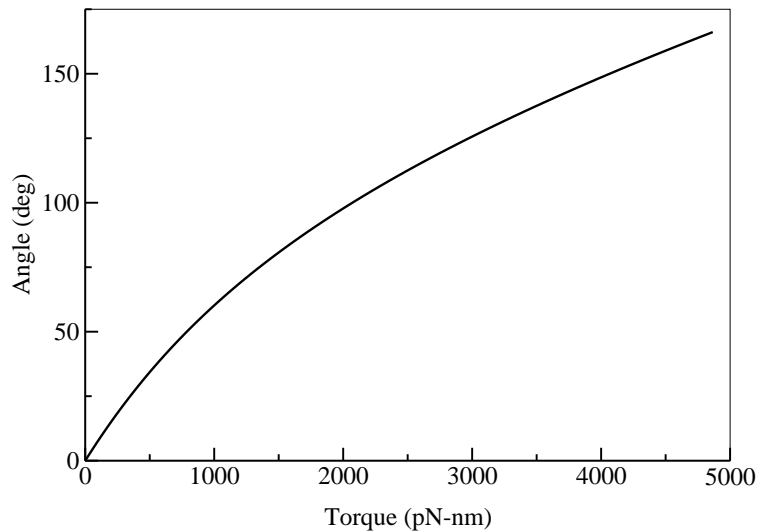


FIG. 1: Compliance curve. The graph shows the angular displacement, $\theta - \theta_L$, between the rotor and the load as a function of the rotor torque. The non linear spring behavior follows approximately the experimental measurement in reference [3]. The curve corresponds to the function $F(x) - F(0)$ used in our simulations.

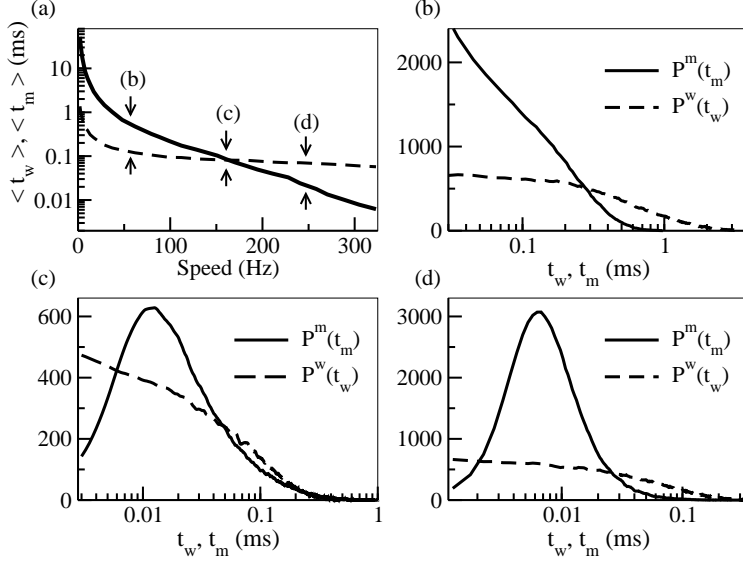


FIG. 2: Waiting-time and moving-time statistic. (a) The average waiting-time (dashed line) and moving-time (solid line) averaged over 500 revolutions as a function of the rotational speed for $N=1$. With increasing speed, the averaged waiting-time slowly decreases from 1ms to 0.1ms while the average moving-time decreases much faster over four orders of magnitude, from roughly 50ms to 0.005ms. The vertical arrows labeled with the letters (b), (c), and (d), indicate the points where the t_w and t_m distributions are shown in the corresponding figures (b), (c), and (d). The value of the load is 14, 1, and $0.1\text{pN}\cdot\text{nm}\cdot\text{s}\cdot\text{rad}^{-1}$, for (b), (c), and (d) respectively. Probability distributions P^m for t_m are shown by solid lines and P^w for t_w are shown by dashed lines. The waiting-times are exponentially distributed in all load range. The moving-times show peaked distributions. The peak at high load is partially hidden by a flat region for small t_w , as a consequence of the rotor fluctuations.

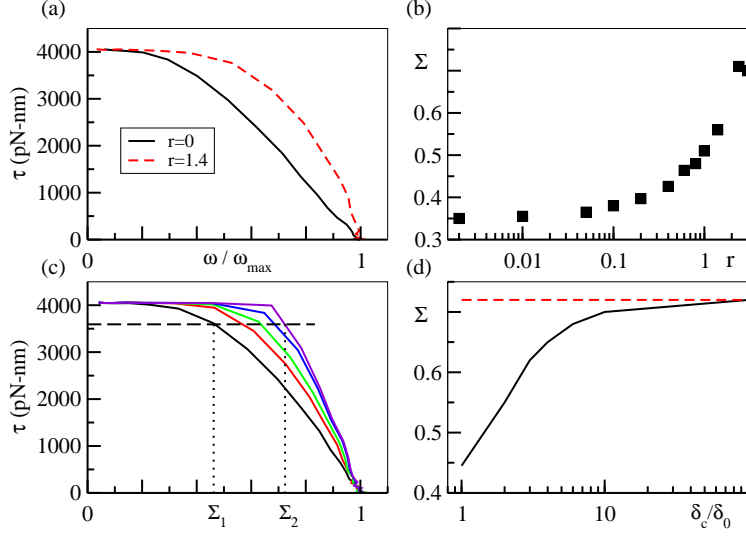


FIG. 3: Dependence of the knee speed ω_n on $r \equiv k_+/k_-$ and on the cutoff δ_c for the symmetric potential with a parabolic bottom. (a) Motor torque as a function of the normalized angular speed for two different values of r : $r = 0$ (black solid line), and $r = 1.4$ (red dashed line). Different from the V-shaped potential, there is a small plateau regime even for $r = 0$. (b) $\Sigma \equiv \omega_n / \omega_{max}$ as a function of r . (c) Torque-speed curves for different values of the cutoff δ_c . Black, red, green, blue, and violet lines correspond to values of δ_c of 1, 2, 3, 6, $100\delta_0$ respectively. Σ_1 and Σ_2 correspond to the values of Σ for $\delta_c = \delta_0$ and $\delta_c = 100\delta_0$ respectively. (d) Σ as a function of the ratio δ_c / δ_0 shown as the black solid line. The red dashed line corresponds to the asymptotic value $\Sigma(\delta_c \rightarrow \infty)$.

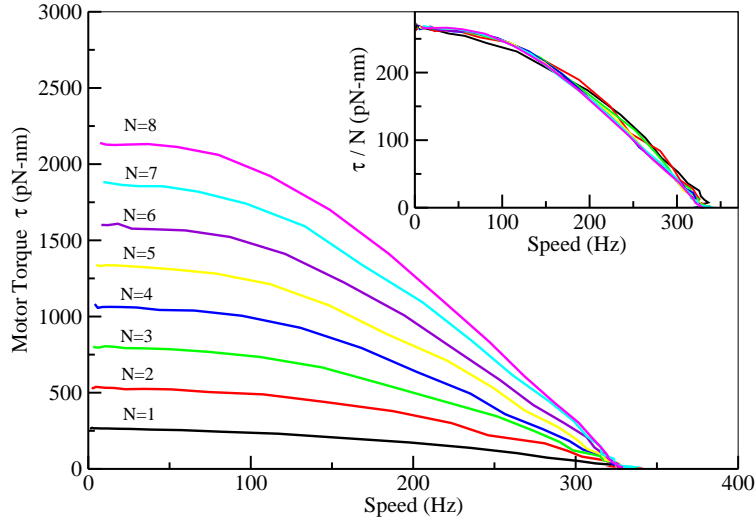


FIG. 4: Torque-speed curves for an asymmetric potential. The torque-speed relationship is very similar to the symmetric potential case. The figure shows the motor torque τ as a function of rotational speed for $N=1, 2, \dots, 8$. For a given value of N the torque is almost constant up to the knee before it decreases roughly linearly. At low speed, the motor torque increases linearly with N . At high speed near zero load all curves collapse to the same maximum speed. These characteristics are apparent in the insert, where the torque per stator τ/N versus ω are shown.

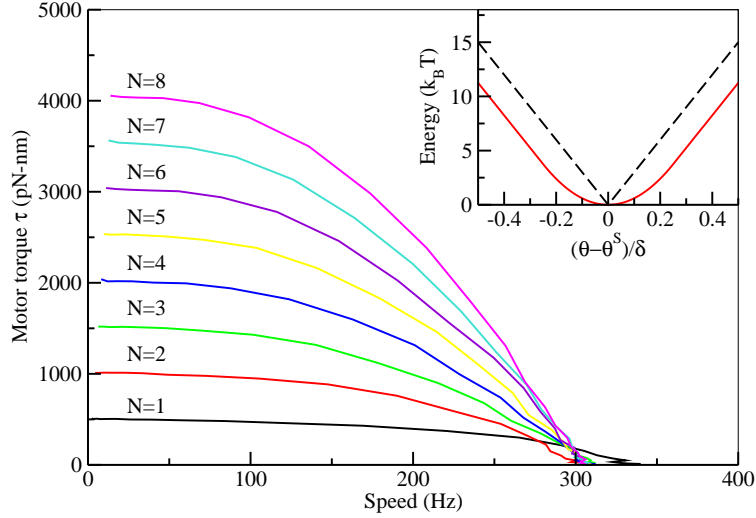


FIG. 5: Torque-speed curves for the symmetric potential with a smooth, parabolic bottom. The behavior is very similar to those observed in the symmetric and asymmetric V-shaped potential cases. The figure shows the motor torque τ as a function of rotational speed for $N= 1, 2, \dots, 8$. For a given value of N the torque is practically constant up to the knee, which is reached at almost the same speed value for different number of stators N , then it decreases linearly with ω . The insert shows the “semi-parabolic” potential (solid red curve) and the symmetric V-shaped potential (dashed black curve) for comparison.

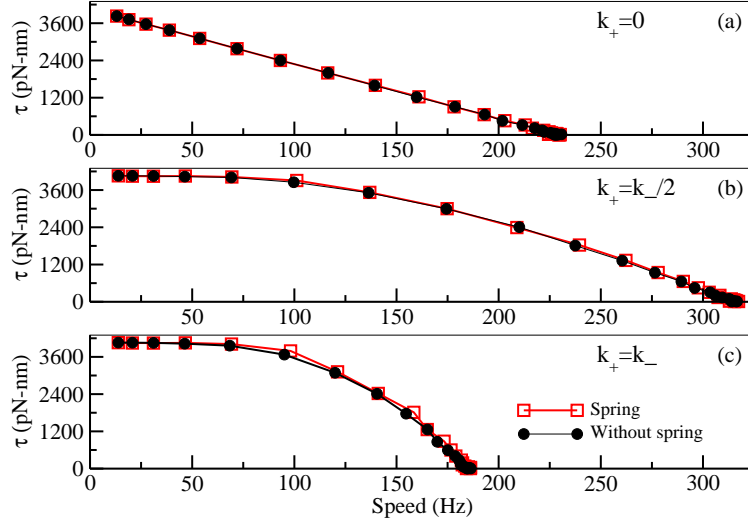


FIG. 6: Independence of the torque-speed characteristics on the load-rotor spring. Torques-speed curves ($N = 8$) with spring (dotted lines) and without spring (squared lines) show almost identical behavior. Instead, the concavity of the torque-speed curve depends on the stator jump rate ratio $r = k_+/k_-$: (a) $r = 0$, (b) $r = 0.5$, and (c) $r = 1$.

Quantity	Value	Comment
ξ_R	$0.002\text{pN}\cdot\text{nm}\cdot\text{s}\cdot\text{rad}^{-1}$	Estimated from [2]
ξ_L	$\approx (0.002\text{-}50)\text{pN}\cdot\text{nm}\cdot\text{s}\cdot\text{rad}^{-1}$	-
δ	$2\pi/26$	From Ref. [6]
δ_0	$\delta/2$	-
T_0	295.85K	Room temperature
τ_0	505pN-nm	Typical value
τ^+	$15K_B\text{T}/0.95\delta$	Typical value
τ^-	$15K_B\text{T}/0.05\delta$	Typical value
k_+ (symm. case)	12000s^{-1}	Fitting data
k_- (symm. case)	$2k_+$	From theory
k_+ (asymm. case)	10000s^{-1}	Fitting data
k_- (asymm. case)	$20k_+$	From theory
κ_0	$400\text{pN}\cdot\text{nm}\cdot\text{rad}^{-1}$	From Ref. [3]
κ_1	$4000\text{pN}\cdot\text{nm}\cdot\text{rad}^{-1}$	From Ref. [3]
$(\theta - \theta_L)_0$	$2\pi/3$	From Ref. [3]
$\Delta(\theta - \theta_L)$	$2\pi/7$	From Ref. [3]
$\Delta\theta_0$	δ_0	-

TABLE I: Parameters used in the calculation.